applied sciences

MDPI

Article

Research on Cooling and Hazardous Gas Dilution Performance of Underground Mining Culvert Ventilation System

Yexian Liu [1], Zhenlei Zhu [1], Hongtao Wang [1], Zhaobiao Luan [1], Delong Meng [1], Qiang Li [1], Zhenneng Lu [2] and Cantao Ye [2,*]

[1] Shandong Energy Group Xibei Mining Co., Ltd., Xi'an 710021, China
[2] Guangzhou Institute of Energy Conversion, Chinese Academy of Sciences, Guangzhou 510640, China
* Correspondence: yect@ms.giec.ac.cn

Abstract

The ventilation system of a mine determines the comfort and safety of the underground working environment. Although many studies have been devoted to reducing the impact of underground heat damage, there are still few comprehensive studies or optimizations aimed at simultaneously considering heat damage prevention and control, exhaust of mechanical equipment, and methane leakage. To address this knowledge gap, a mine ventilation model was built and validated to analyze the impact of different numbers of top fans on the distribution characteristics of temperature and gas mass fraction. Subsequently, the impact of different blowing duct inlet temperatures and velocities on the capacity to cool and dilute hazardous gases was investigated. Finally, a comprehensive coefficient that removes the effect of dimension was proposed for evaluating the cooling and dilution performance of different top fan cases. The results show that a top fan is the most advantageous for cooling the mine, but has a poor ability to dilute hazardous gases. Three top fans have the best performance for diluting hazardous gases, which leads to some degree of heat diffusion, but obtains the maximum total comprehensive coefficient of 0.71246.

Keywords: mine ventilation system; mine comfort and safety; thermal management; multi-species transport

Check for updates

Academic Editor: Nikolaos Koukouzas

Received: 21 April 2026
Revised: 26 May 2026
Accepted: 4 June 2026
Published: 5 June 2026

Copyright: © 2026 by the authors. Licensee MDPI, Basel, Switzerland. This article is an open access article distributed under the terms and conditions of the Creative Commons Attribution (CC BY) license.

1. Introduction

Although most countries are actively developing renewable energy sources, it remains challenging to eliminate reliance on traditional energy sources such as coal, oil, and natural gas in the short term. Globally, most coal is extracted through underground mining, with up to 85% of coal mines in China originating from underground mining [1]. According to statistics, the coal reserves within 2000 m vertical depth are 557 trillion tons, respectively [2]. As the extraction of coal from shallow mines decreases, the proportion of deep mines continues to rise. In the next 10–15 years, 53% of coal mines in China will be mined to a depth of more than 1000 m [3]. With the gradual increase in the depth of mining, the problem of high-temperature heat damage caused by the geothermal heat of the mine is becoming more serious [4]. According to statistics, at a mine depth of 600 m in the Zhuji mine in China, the temperature of the rock wall around the mine tunnel reached 47 °C [5]. Concurrently, in deep underground mines, cooling systems can consume up to 25 percent of the total electricity [6], and the high cooling costs associated with deep mines represent a prevalent issue in current mine cooling methods, thereby limiting the depth of coal extraction. Furthermore, the environment of underground mines is complex and

hazardous, with factors such as high temperatures [7], toxic gases [8], and dust [9] posing significant threats to the health and safety of workers.

Currently, cooling technologies for deep mines encompass mechanical refrigeration [10], water injection cooling [11], and phase change cooling [12], etc. Mechanical refrigeration can provide more cooling capacity to suppress high mine temperatures than direct ventilation, but it often comes with higher energy consumption [13]. Wang et al. [14] optimized the pump power at each position in a mechanical refrigeration system for a deep mine, and the total energy consumption was reduced by 25.79%. Compared to mechanical refrigeration, water injection cooling and phase change cooling (ice production) [15] are more effective in lowering the temperature of the surrounding rock and have lower cooling losses. However, these cooling technologies invariably rely on rational ventilation arrangements to ensure the safety of the mine environment, including parameters such as temperature, oxygen concentration, and hazardous gas concentration.

Indeed, rational underground mine ventilation arrangements can effectively dilute hazardous gas concentrations and enable refined management of airflow and thermal distribution, while improving worker comfort. Bascompta et al. [16] proposed a geographic information system (GIS) to quantitatively record the gas concentration of the entire mine to analyze the ventilation demand at each location. Chen et al. [17] constructed a simulation model of mine ventilation with a spray cooling system and optimized the spraying scheme, which showed that the maximum temperature of the walkway was only 27 °C when the water temperature was 13 °C and the spraying spacing was 10 m. Wang et al. [18] conducted a study on the local ventilation of the head and neck of workers; the results showed that the local ventilation of a deflected jet can obtain a larger ventilation area and effectively improve human comfort. Habibi et al. [19] calibrated a ventilation model of a real coal mine culvert and improved its scheme by simulating the airflow and heating conditions, which ultimately reduced the operating costs, and showed that the changes in the operating conditions of the surface fans reduced their power consumption by about 17%. However, research that comprehensively considers the combined effects of surrounding rock thermal conditions, gas leakage, mechanical heat load, and exhaust emissions on underground air conditions and cooling capacity remains scarce. Although the study by Kurnia et al. [20] provides a detailed discussion on the management of hazardous gases, it does not account for oxygen consumption by mechanical equipment exhaust. Additionally, the excessively high air temperatures and mechanical equipment temperatures reported in their findings do not comply with the requirements outlined in the Coal Mine Safety Regulations [21].

In summary, based on the research of Kurnia et al. [20] and the Coal Mine Safety Regulations, this study will employ Computational Fluid Dynamics (CFD) numerical simulation to analyze the working environment and cooling requirements in deep mines, considering factors such as the heat load from surrounding rock and mechanical equipment, gas leakage, exhaust emissions and oxygen consumption from mechanical equipment. This research will further refine the description of the underground mine environment in a virtual model, providing preliminary data and a model foundation for subsequent online monitoring of the mine environment and the development of a digital twin model.

2. Model Description and Validation

2.1. Description of Underground Mining Areas

The structure of the underground mine is shown in Figure 1. The model is divided into two parts: the mining face culvert and the main culvert. Airflow flows freely through the main culvert, and a blowing duct is used to supply cool air to the mining face for cooling and diluting leaked methane. Top fans are used to effectively prevent hot or hazardous gases from collecting at the top of the culvert. A shuttle car and a continuous miner are

placed inside the mining face culvert as the sources of heat, hazardous gas release and oxygen consumption. The tailpipe outlets are set on the top side of the tail section of the shuttle car and continuous miner to facilitate the release of exhaust gases into the main culvert. More detailed parameters for the underground mine studied in this paper can be found in Table 1.

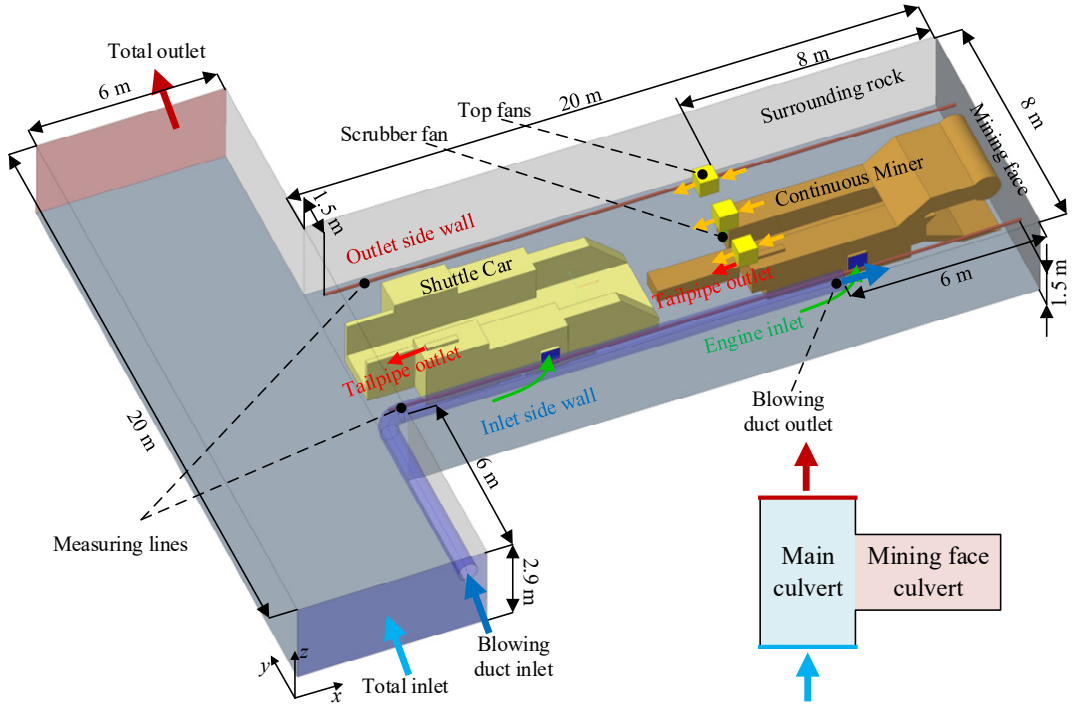


Figure 1. The structure for an underground mine.

Table 1. The detailed parameters for underground mine.

Items	Parameters	Value
Mine culvert	W × L × H (m × m × m)	6 × 20 × 2.9
Mining face culvert	W × L × H (m × m × m)	20 × 8 × 2.9
Top fan	W × L × H (m × m × m)	0.6 × 0.6 × 0.6
	Distance to mining face (m)	8
Blowing duct	Diameter (m)	0.6
	Distance to side wall (m)	0.3
	Distance from outlet to mining face (m)	6
Tailpipe outlet	L × H (m × m)	0.2 × 0.1
Engine inlet	W × H (m × m)	0.6 × 0.6
Continuous miner	Distance to mining face (m)	0.15
	Size (m)	Ref. [20]
Shuttle car	Distance to mining face (m)	11
	Size (m)	Ref. [20]
Measuring lines	Length (m)	20
	Distance to bottom (m)	1.5
	Distance to side wall (m)	1.5
Scrubber fan	L × H (m × m)	0.5 × 0.5

2.2. Model Formulations and Boundary Conditions

2.2.1. Governing Equation

To investigate the distribution of hazardous gases and temperature in the underground mine, the cfMesh v1.1.2 and OpenFOAM v2512 software were used to establish the mesh model and simulation model, respectively. The numerical simulation follows the best

practices for mine gas dispersion CFD analysis as summarized in Ref. [22]. The continuity equation can be described as follows:

$$\frac{\partial u}{\partial x} + \frac{\partial v}{\partial y} + \frac{\partial w}{\partial z} = 0 \tag{1}$$

where u, v and w are the velocities in the x, y and z directions, respectively.

The momentum conservation equation is described as follows:

$$\nabla \cdot \left(\rho_{mix} \vec{V}\vec{V} \right) = -\nabla P + \rho_{mix} \vec{g} + \nabla \cdot (\mu + \mu_t) \left[\left(\nabla \vec{V} + \nabla \vec{V}^T \right) + \frac{2}{3} \nabla \cdot \vec{V} I - \rho_{mix} \kappa I \right] \tag{2}$$

where $\vec{V}$ is the velocity vector; μ and μ_t are the dynamic viscosity and turbulent viscosity, respectively; κ is the turbulent kinetic energy; I is the unit tensor; ρ_{mix} is the mixture species density; P is the pressure; and $\vec{g}$ is the gravity vector.

The energy conservation equation is described as follows:

$$\nabla \cdot \left(\rho_{mix} \vec{V} T \right) = \nabla \cdot \left(\frac{\lambda}{c_p} + \frac{\mu_t}{Pr_t} \right) \nabla T \tag{3}$$

where T is the temperature; λ and c_p are the thermal conductivity of the fluid and the specific heat capacity, respectively; and Pr_t is the turbulent Prandtl number with a default value of 0.85 in the OpenFOAM v2512 software.

The convection–diffusion conservation equation is described as follows:

$$\nabla \cdot \left(\rho_{mix} \vec{V} Y_i \right) = -\nabla \cdot \vec{J_i} \tag{4}$$

where Y_i is the local mass fraction of each species; $\vec{J_i}$ is the diffusion flux of species i, which can be described as follows:

$$\vec{J_i} = -\left(\rho_{mix} D_{i,m} + \frac{\mu_t}{Sc_t} \right) \nabla Y_i - D_{T,i} \frac{\Delta T}{T} \tag{5}$$

where $D_{i,m}$ is the mass diffusion coefficient for the species in the mixture; $D_{T,i}$ is the thermal diffusion coefficient; Sc_t is the turbulent Schmidt number and the default value is 0.7.

2.2.2. Turbulence Model

The standard κ-ε model is used in this study. The choice of this model is justified by the following considerations: (1) it has been widely validated for high-Reynolds-number forced convection flows in underground mine tunnels, with prediction errors typically less than 5% for velocity and temperature fields; (2) compared to the RNG κ-ε and κ-ε SST models, it offers 30% higher computational efficiency while maintaining sufficient accuracy for global flow and thermal distribution analysis; and (3) this study focuses on the overall performance of the ventilation system rather than local boundary layer details, making the standard κ-ε model the most appropriate choice. The model equations are as follows:

$$\nabla \cdot \left(\rho_{mix} \vec{V} \kappa \right) = \nabla \cdot \left[\left(\mu + \frac{\mu_t}{\sigma_\kappa} \right) \nabla \kappa \right] + G_\kappa + G_b - \rho_{mix} \varepsilon \tag{6}$$

$$\nabla \cdot \left(\rho_{mix} \vec{V} \varepsilon \right) = \nabla \cdot \left[\left(\mu + \frac{\mu_t}{\sigma_\varepsilon} \right) \nabla \varepsilon \right] + C_{1\varepsilon} \frac{\varepsilon}{\kappa} (G_\kappa + C_{3\varepsilon} G_b) - C_{2\varepsilon} \frac{\rho_{mix} \varepsilon^2}{\kappa} \tag{7}$$

where κ and ε are the turbulent kinetic energy and the dissipation rate of turbulent pulsation kinetic energy, respectively; G_κ is the turbulent kinetic energy at the mean velocity

gradient and $G_\kappa = \rho_{mix}\overline{u_i'u_j'}\frac{\partial u_j}{\partial x_i}$, in which i and j represent the x-, y- or z-axis; μ_t is the turbulent viscosity, $\mu_t = \rho C_\mu \frac{\kappa^2}{\varepsilon}$; G_b is the turbulent kinetic energy generated by buoyancy, $G_b = \beta g_i \frac{\mu_t}{Pr_t}\frac{\partial T}{\partial x_i}$; Pr is the Prandtl number, Pr_t = 0.85; β is the expansion coefficient, $\beta = -\frac{1}{\rho}\left(\frac{\partial \rho}{\partial T}\right)_P$; $C_{1\varepsilon}$, $C_{2\varepsilon}$, $C_{3\varepsilon}$, C_μ, σ_k and σ_ε are constants in the standard κ-ε model.

Pressure–velocity coupling is achieved using the SIMPLE algorithm. The momentum, energy and species transport equations are discretized using the second-order upwind scheme. Standard wall functions are employed for near-wall treatment, with the first layer mesh height adjusted to ensure $y^+ \approx 30$. The maximum mesh size in the main flow region is 20 cm, and the near-wall region is refined to 5 cm.

2.2.3. Mixture Species Properties Formulations

The density of the mixture is described as follows:

$$\rho_{mix} = \frac{pM}{RT} \tag{8}$$

where R is the universal gas constant, and M is the molar mass of the mixture, which can be described as follows:

$$M = \left[\sum_{i=1}^{N}\frac{Y_i}{M_i}\right]^{-1} \tag{9}$$

where M_i is the molar mass of each species i, including O_2, CO_2, NO_2, N_2, H_2O and CH_4.

The specific heat capacity of the mixture is described as follows:

$$C_p = \sum_{i=1}^{N} Y_i C_{p,i} \tag{10}$$

where $c_{p,i}$ is the specific heat capacity of species i.

The dynamic viscosity of the mixture is described as follows:

$$\mu = \frac{\sum_{i=1}^{N} X_i \mu_i}{\sum_{i=1}^{N} X_i V_i} \tag{11}$$

where μ_i, V_i and X_i are the dynamic viscosity, mole volume and mole fraction of species i, respectively.

2.2.4. Diesel Engine Combustion

Both the continuous miner and the shuttle car rely on diesel engines for power; the chemical equation for diesel combustion is described as follows:

$$C_{16}H_{34} + \frac{49}{2}O_2 \rightarrow 16CO_2 + 17H_2O \tag{12}$$

In this study, the continuous miner and the shuttle car have diesel engines with a horsepower of 381 hp and 229 hp, respectively, and the diesel consumption rate is 0.416 L/hp·h. In addition, it is stated in specification MT220-1990 [23] that the emission rate of NO_X from a mine diesel engine cannot exceed 800 ppm. Combining the above conditions and Equation (12), the air consumption, tailpipe emission rates and mass fractions of each species can be calculated, and the calculated results as boundary condition data are shown in Table 2.

Table 2. Calculated boundary condition parameters.

Items	Boundary Conditions	Parameters	Values
Total inlet	Velocity inlet	Velocity (m/s)	2
		Temperature (°C)	25
		Mass fraction	0.2317 CO_2 0.7683 N_2
Total outlet	Pressure outlet (Prevent reverse flow)	Pressure (Pa)	101,325
Blowing duct inlet	Velocity inlet	Velocity (m/s)	8–16
		Temperature (°C)	5–25
		Mass fraction	0.2317 CO_2 0.7683 N_2
Surrounding rock	Wall	Temperature (°C)	31
Continuous miner	Wall	Heat flux (W/m^2)	2732
Continuous miner tailpipe outlet	Mass flow inlet	Mass flow rate (kg/s)	0.5061
		Temperature (°C)	77
		Mass fraction	0.6946 N_2 0.1860 CO_2 0.1192 H_2O 0.0002 NO_2
Continuous miner engine inlet	Out fan	Volume flow rate (m^3/s)	0.3929
Scrubber fan	Fan	Velocity (m/s)	10
		Pressure drops (Pa)	170
Shuttle car	Wall	Heat flux (W/m^2)	1458
Shuttle car tailpipe outlet	Mass flow inlet	Mass flow rate (kg/s)	0.3042
		Temperature (°C)	77
		Mass fraction	0.6946 N_2 0.1860 CO_2 0.1192 H_2O 0.0002 NO_2
Shuttle car engine inlet	Out fan	Volume flow rate (m^3/s)	0.2361
Mining face	Discrete perforated wall	Temperature (°C)	31
		Number of holes	14
		Diameter of holes (m)	0.1
		Mass flow rate (kg/s)	14 × 0.00135
		Mass fraction	1.00 CH_4
Top fan	Fan	Velocity (m/s)	10
		Pressure drops (Pa)	190

2.2.5. Boundary Conditions

In the simulation, the following assumptions are used: (1) The walls of continuous miner, the shuttle car and the surrounding rock are considered as heat sources. (2) The average temperature in the mine tunnel is below 50 °C, and radiant heat transfer accounts for less than 5% of the total heat transfer. Since this study focuses on the forced convection-dominated flow and temperature fields, the effect of radiant heat transfer can be neglected. (3) The maximum air velocity in this study is 16 m/s, corresponding to a Mach number less than 0.05, and the density change caused by compressibility is less than 0.1%, which has a negligible impact on the simulation results. (4) The length of the blowing duct is only 20 m with good thermal insulation, resulting in a cooling loss rate below 3%, while the along-track resistance causes a velocity change of less than 0.2 m/s, which does not affect the relative performance comparison between different cases. Four top fan cases are defined in this study: Case 1: no top fan; Case 2: one top fan; Case 3: two top fans; Case 4: three top fans. The boundary conditions can be found in Table 2.

2.3. Performance Indicators

To analyze the effects of different blowing inlet temperatures and velocities, the average temperature and species mass fractions of the pedestrian passage (measured along two lines,

as shown in Figure 1) are employed. To evaluate the performance of the mine ventilation system, a comprehensive coefficient is applied that considers the average temperature, maximum temperature, energy consumption and the mass fraction of each gas.

The temperature and species mass fractions of the pedestrian passage were calculated using the ParaView 6.0 software.

In addition, the temperature and species mass fractions need to be within the permissible ranges based on the Coal Mine Safety Regulations [21], as shown in Table 3.

Table 3. Requirements for temperature and species mass fractions.

Items	Requirements
Temperature (°C)	30
CH_4	<0.276%
CO_2	<0.759%
NO_2	<0.000397%
O_2	>22%

(1) Energy Consumption Calculation

Energy consumption evaluates the necessary energy for different operational parameters, and it can be calculated as follows:

$$P_{total} = P_{topfan} + P_{cooling} \tag{13}$$

where P_{total} represents the total power of the mine ventilation system; P_{topfan} represents the power of the top fans; and $P_{cooling}$ is the power required to make the blowing duct low-temperature fluid. They can be calculated as follows:

$$\begin{cases} P_{topfan} = \frac{nKQp_{wind}}{\eta_1\eta_2} \\ P_{cooling} = \frac{Q}{COP} = \frac{c_p q_v \rho (T_{duct} - T_{amb})}{COP} \end{cases} \tag{14}$$

where n is the number of top fans; K is the motor capacity factor, assumed to be 1.2; Q is the volume flow rate; p_{wind} is the wind pressure, $p_{wind} = \frac{1}{2}\rho v^2$; η_1 and η_2 are the fan efficiency and the mechanical drive efficiency, respectively, η_1 = 0.75 and η_2 = 1; COP is the coefficient of cooling, which is assumed to be 3.5 in this study; T_{duct} and T_{amb} are the temperatures of the duct outlet and the ambient, in which T_{amb} is assumed to be 25 °C; c_p and ρ are assumed to be the heat capacity and density of air, c_p = 1.005 kJ/kg and ρ = 1.293 kg/m^3.

The energy consumption of the scrubber fan is not included in the calculation because its operating parameters (volume flow rate 0.3929 m^3/s, pressure drop 170 Pa) are constant across all cases, and thus do not affect the relative performance comparison between different top fan configurations and blowing duct parameters.

(2) Comprehensive Coefficient Definition

To eliminate the dimensional effect of different indicators and achieve a unified evaluation of cooling performance, energy consumption and hazardous gas dilution capacity, this study proposes three types of dimensionless comprehensive coefficients: the temperature–power comprehensive coefficient, the hazardous gas dilution comprehensive coefficient and the total comprehensive coefficient. In this study, the comprehensive coefficient (η) is proposed for evaluating the cooling ability, power consumption and the ability to dilute hazardous gases of the mine ventilation system, which can eliminate the effect of different scales between indicators. η_k can be defined as follows:

$$\eta = \sum_{j=1}^{m} \omega_j y_{ij} \tag{15}$$

where η is divided into three types: the temperature–power comprehensive coefficient ($\eta_{cooling}$), the hazardous gases dilution comprehensive coefficient (η_{gases}) and the total comprehensive coefficient (η_{total}); m is the number of indicators: $\eta_{cooling}$: m = 2 (temperature and power), η_{gases}: m = 4 (mass fractions of O_2, CO_2, NO_2, CH_4), η_{total}: m = 6 (temperature, power and mass fractions of O_2, CO_2, NO_2, CH_4); ω_j is the weight of each indicator; and y_{ij} is the normalized value of the j-th indicator in each of the i-th samples.

Indicator normalization and weight calculation based on the coefficient of variation can be described as follows:

$$\begin{cases} y_{ij}^{+} = \frac{x_{ij} - \min(X_j)}{\max(X_j) - \min(X_j)} \\ y_{ij}^{-} = \frac{\max(X_j) - x_{ij}}{\max(X_j) - \min(X_j)} \\ \omega_j = \frac{V_j}{\sum_{j=1}^{m} V_j} \end{cases} \tag{16}$$

where y_{ij}^{+} and y_{ij}^{-} are the normalized values for positive (bigger is better) and negative (smaller is better) indicators, respectively, with the mass fraction of O_2 as the positive indicator and the rest as negative indicators; x_{ij} represents the j-th indicator in each of the i-th samples; X_j represents all samples for the j-th indicator; V_j represents the coefficient of variation in the j-th indicator, which can be described as follows:

$$\begin{cases} V_j = \frac{S_j}{\overline{Y}_j} \\ \overline{Y}_j = \frac{1}{n} \sum_{i=1}^{n} y_{ij} \\ S_j = \sqrt{\frac{1}{n-1} \sum_{i=1}^{n} \left(y_{ij} - \overline{Y}_j\right)^2} \end{cases} \tag{17}$$

where S_j and $\overline{Y}_j$ are the standard deviation and average value of the j-th indicator, respectively; n is the number of samples for the j-th indicator.

2.4. Model Validation

The results derived from Kurnia et al. [20] are used as the target for model validation in this study. It should be noted that the model in Ref. [20] has been validated against field measurement data from an Australian underground coal mine, with temperature and gas concentration errors within the acceptable engineering range. Compared to the model in this study, the width of the mining face culvert in the validated model is 6 m, and the engine inlet, top fans and the methane leakage from the mining face are not included in the model. The mesh number level of the validated model is consistent with that of Ref. [20], and the number of mesh elements is 2,563,964. The validated conditions are: the blowing inlet velocity is 12 m/s and the temperature is 25 °C. As shown in Figure 2, the maximum absolute errors of the oxygen mass fraction and the cross-sectional average temperature are 0.009 and 2.7 °C, respectively, indicating that the model simulation results are accurate.

Based on the model descriptions in Section 2.1 to Section 2.3, mesh independence was tested for each of the four top fan cases. In the simulations, the blowing duct inlet velocity and temperature were kept at 12 m/s and 15 °C, respectively. As shown in Figure 3, it could be seen that when the mesh number was larger than 3,000,000, none of the average temperature changes were greater than 0.2 °C if the mesh number continued to increase. To further ensure the reliability of the simulation results, we also performed mesh independence tests for velocity and CH_4 mass fraction. When the mesh number increased from 3 million to 4 million, the average velocity in the pedestrian passage changed by

0.08 m/s with a relative error of 2.1%, and the average CH_4 mass fraction changed by 3.2×10^6 with a relative error of 1.8%. Both changes are within the acceptable engineering accuracy range.

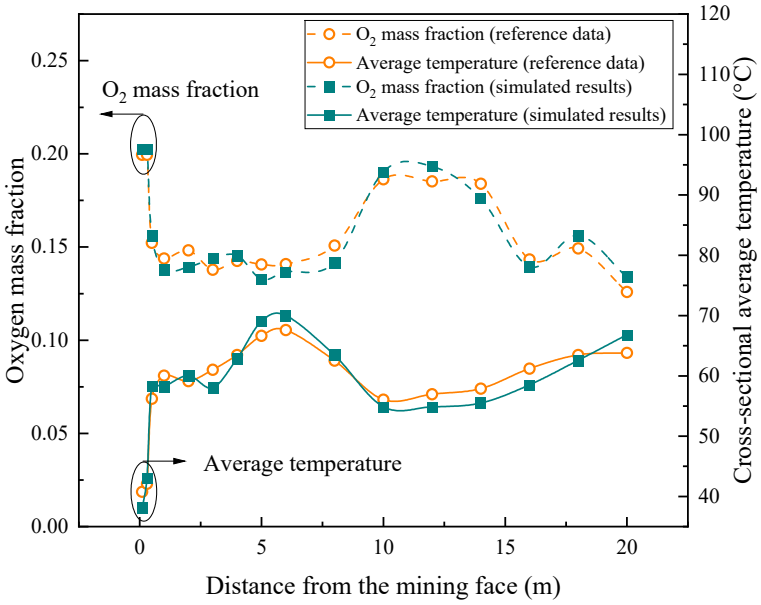


Figure 2. Absolute error distribution of simulation results, reference data from ref. [20].

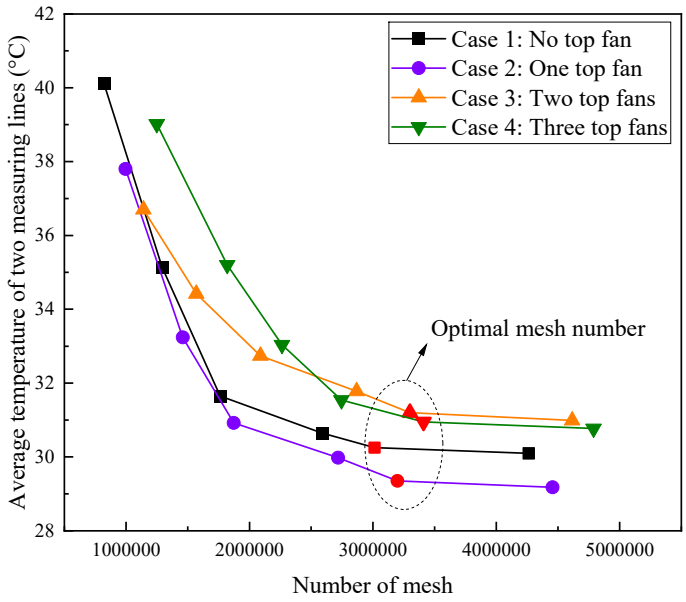


Figure 3. Test of mesh independence.

Therefore, the number of meshes for Case 1, Case 2, Case 3 and Case 4 in the subsequent study were 3,014,500, 3,199,541, 3,300,633 and 3,411,571 (red points), respectively. The simulation was considered converged when the residuals of the continuity equation were less than 1.0×10^6, those of the energy equation were less than 1.0×10^7, and those of all species transport equations were less than 1.0×10^6. Each case took approximately 12 h to run on an Intel Xeon Gold 6248R processor (24 cores, 3.0 GHz).

2.5. Flowchart

The working flowchart of this study is shown in Figure 4. With the validated 3D model, the thermal distribution and species distribution are first discussed for the base operating

condition (no top fan, with the blowing inlet temperature and velocity set to 15 °C and 12 m/s). Then the impacts of the top fans and the blowing duct supply air conditions on the ventilation performance are discussed by using the top fan number, blowing duct velocity and temperature as control variables. Finally, the suitable operating data range for the mine ventilation system is obtained.

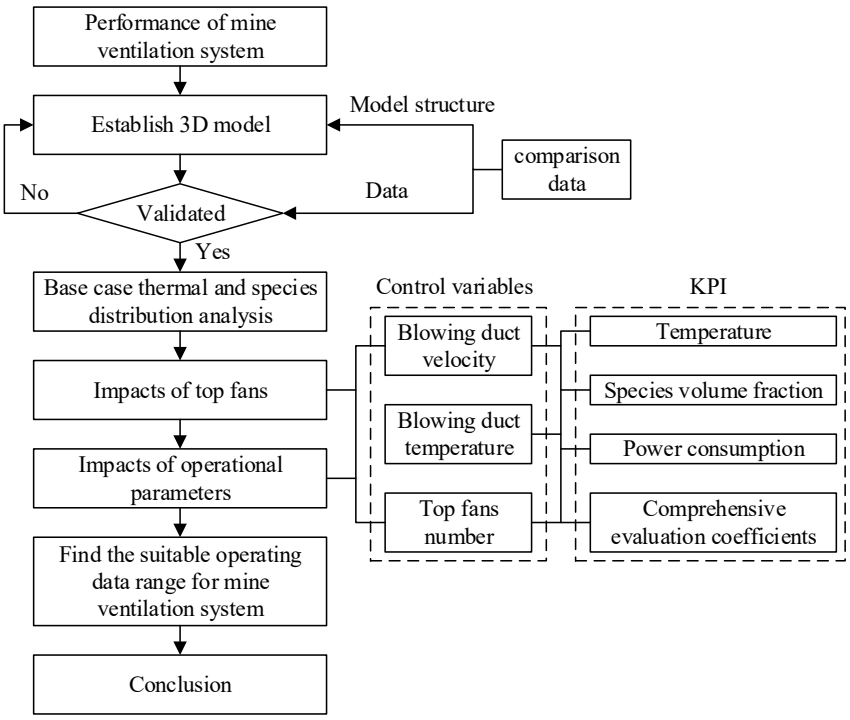


Figure 4. Flowchart of this paper, comparison data from ref. [20].

3. Results

3.1. Temperature and Species Distribution for Different Top Fan Number

Figure 5 shows the temperature distribution of the four top fan cases for the base operating condition. The results show that the high-temperature region at the mining face culvert's top in Case 2 is the smallest, followed by Cases 3, 1, and 4. This is because the single top fan in Case 2 is located directly above the center of the mining face culvert, forming a directional exhaust channel that efficiently discharges the high-temperature fluid from the center of the mining face to the main culvert. In contrast, the three top fans in Case 4 are evenly distributed along the width of the culvert, generating strong turbulence that causes the high-temperature fluid to diffuse to both sides of the culvert instead of being discharged directly. This prevents the formation of a concentrated exhaust channel and increases the heat retention time, resulting in a higher average temperature than in Case 2. This phenomenon is also consistent with the temperature distribution contour map in Figure 5.

In addition, there is no obvious local high-temperature phenomenon on either side of the equipment in Case 2. This is because the high-temperature fluids are effectively accelerated by the top fan in the center of the mining face culvert. Both Cases 1 and 4 have local high temperatures at the inlet side. This is because the fluid in the main culvert flows into the mining face culvert through the bottom of the outlet side and moves upward to the top, thereby pushing the hot fluid to shift towards the inlet side. There are local high temperatures on both sides of the equipment in Case 3. This is because the high-temperature fluids in the center are not effectively discharged into the main culvert and are diffused by the influence of the top fans on both sides.

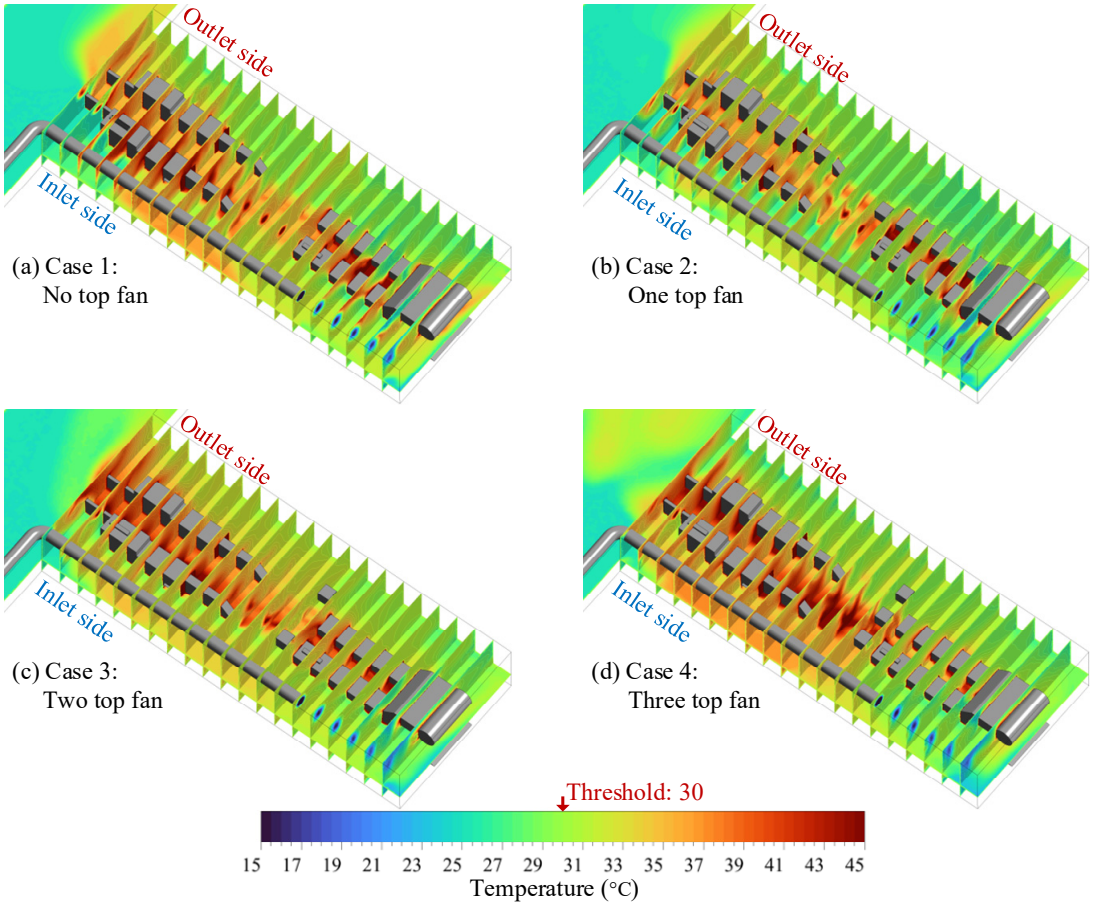


Figure 5. Temperature distribution for different top fan numbers.

The distribution of the O_2 mass fraction under the base operating condition for the four top fan cases is shown in Figure 6. The results show that when the oxygen mass fraction minimum threshold is set at 0.22, Case 4 obtains the largest region of high O_2 mass fraction, followed by Cases 3, 2, and 1. This is because the top fans increase the flow velocity at the mining face culvert's top and then decrease the internal pressure inside the culvert, which drives the flow of gases with a high O_2 mass fraction into the mining face culvert from the main culvert. Significantly, Cases 1, 2, and 3 have lower air mass fractions on the inlet side than on the outlet side, and Case 1 has the largest difference. This is due to the fluid in the main culvert mainly flowing through the bottom of the outlet side into the mining face culvert and gradually flowing to the top, whereas the exhaust gases discharged to the top prevent the fluid with a high O_2 mass fraction from flowing to the inlet side. Moreover, with an increase in the number of top fans, the region of low O_2 mass fraction on the inlet side gradually decreases, and Case 4 eliminates the region of low O_2 mass fraction. This is because the turbulence created by the top fans to some extent promotes the diffusion of the fluid with a high O_2 mass fraction.

The impact of different numbers of top fans on the distribution of CH_4 released from the mining face is shown in Figure 7. In all four top fan cases, CH_4 leaked from the mining face accumulates in the corners of the outlet side. This is because the fluid supplied by the blowing duct creates vortices in the corner after laterally skimming the mining face. In addition, the CH_4 mass fraction gradually decreases as the fluid flows toward the mining face culvert outlet. However, Case 2 has almost no CH_4 on the inlet side; this is due to the low turbulence intensity and effective isolation of the two side regions above the shuttle car and continuous miner in Case 2, which does not promote the diffusion of CH_4. Cases 1, 3, and 4 show CH_4 on both sides of the shuttle car and the continuous miner, with Case 1

resulting from the absence of a top fan to promote internal fluid flow toward the main culvert, and Cases 3 and 4 resulting from excessive turbulence intensity.

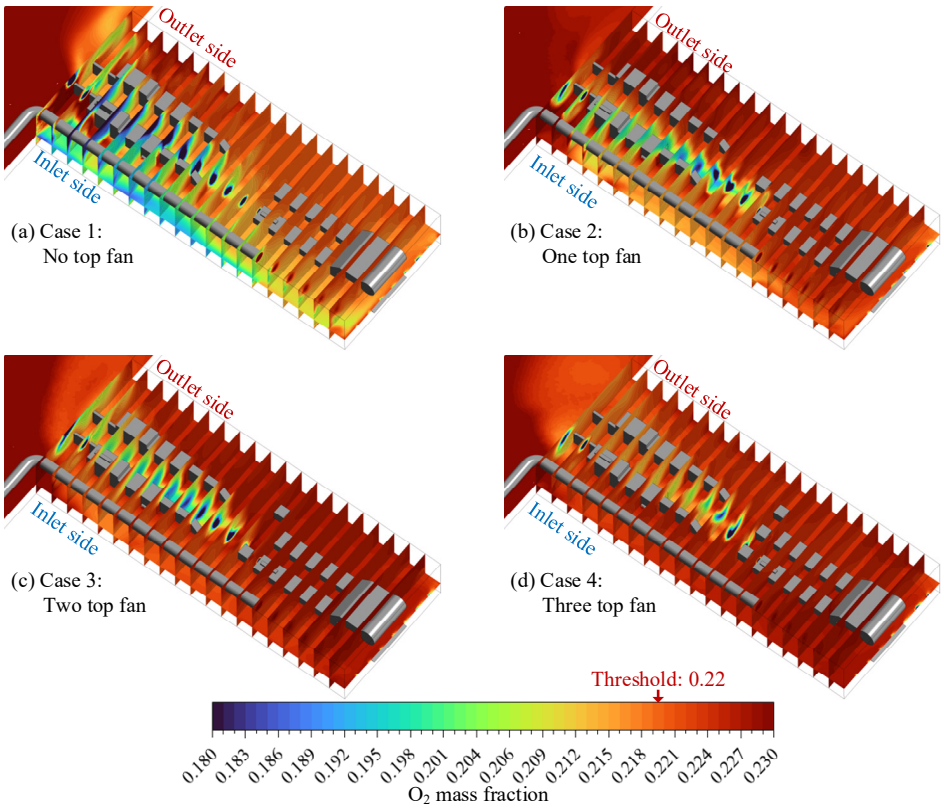


Figure 6. O_2 mass fraction distribution for different top fan number.

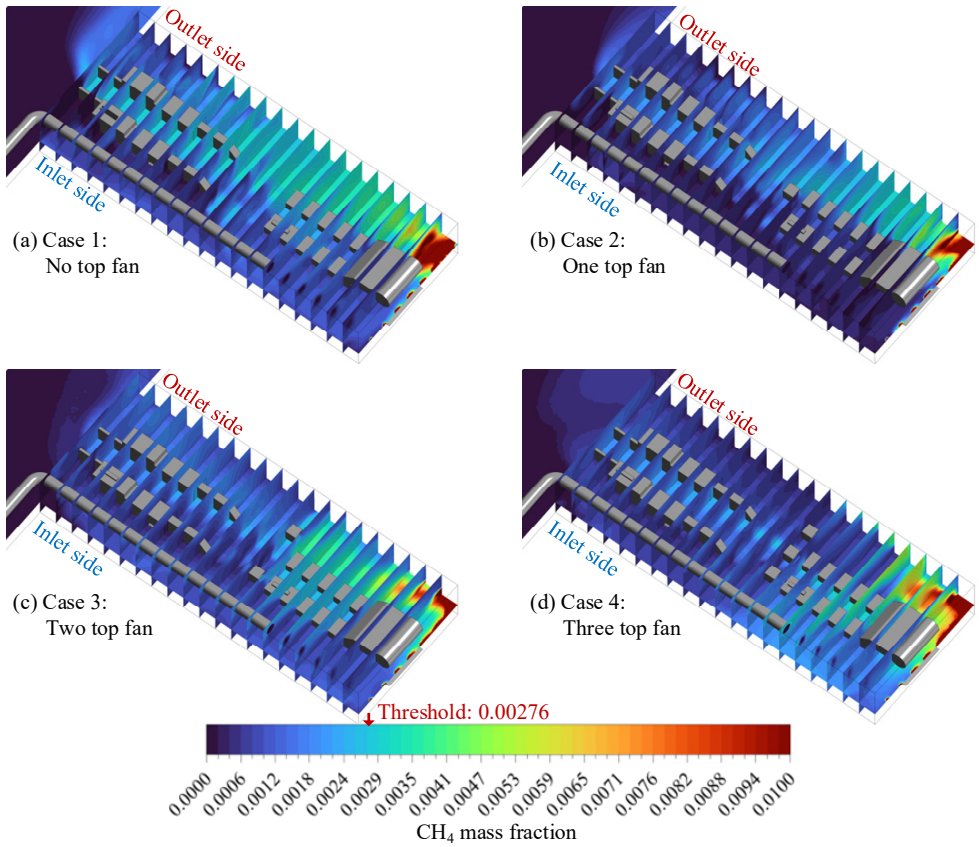


Figure 7. CH_4 mass fraction distribution for different top fan numbers.

The effect of different numbers of top fans on the mass fraction distributions of CO_2 and NO_2 emitted by diesel engines is shown in Figures 8 and 9, respectively. It is clear that the diffusion region of CO_2 is larger than that of NO_2 for each top fan case; this is because the mass fraction of CO_2 in the exhaust gases is much larger than that of NO_2. In addition, the distribution patterns of the two gases are almost the same, differing only in their mass fractions. This is because both CO_2 and NO_2 flow out from the same location and have similar molar masses (CO_2: 44 g/mol; NO_2: 46 g/mol). It is noteworthy that CO_2 and NO_2 in Case 4 have little distribution in front of the tailpipe. However, in Cases 1, 2, and 3, both CO_2 and NO_2 can diffuse to the vicinity of the mining face, with the most severe diffusion occurring in Case 1, followed by Cases 2 and 3. This is because CO_2 and NO_2 have larger molar masses than gases such as oxygen (O_2), nitrogen (N_2), and methane (CH_4). If they are not discharged into the main culvert immediately after the exhaust gas is emitted, CO_2 and NO_2 will deposit at the bottom of the culvert and spread to the mining face with the gas flow entering from the bottom of the mining face culvert.

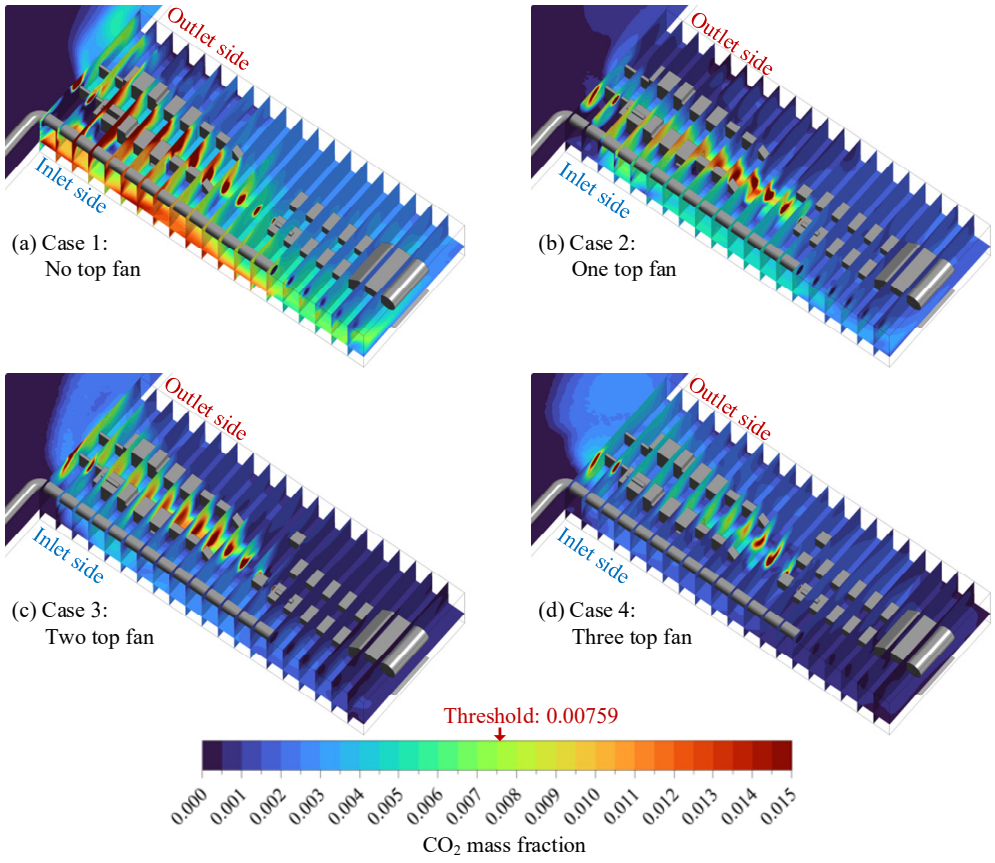


Figure 8. CO_2 mass fraction distribution for different top fan number.

3.2. Impact of Operating Parameters

In order to analyze culvert temperature, energy consumption and the level of dilution of hazardous gases for each top fan case under different operating parameters, the control variable method was adopted to discuss the effects of different blowing duct inlet velocities and temperatures.

The variation in the average temperature with the blowing duct inlet velocity for the different top fan cases is shown in Figure 10. The average temperature decreases with increasing inlet velocity in all cases. For example, in Case 1, the average temperature decreases from 31.1 °C to 29.9 °C with an increase in the inlet velocity from 8 m/s to 16 m/s, which is due to the higher inlet velocity resulting in more cooling capacity. However, the reduction in the average temperature diminishes as the inlet velocity increases. For example,

in Case 2, the average temperature decreases by 0.85 °C when the inlet velocity increases from 8 m/s to 10 m/s, but when the inlet velocity increases from 14 m/s to 16 m/s, the average temperature only decreases by 0.05 °C. It is noteworthy that the lowest average temperatures are obtained at any inlet velocity for Case 2, followed by Cases 1, 4, and 3. For example, when the wind speed is 12 m/s, the average temperatures are 29.35 °C, 30.25 °C, 30.95 °C and 31.20 °C for Cases 2, 1, 4, and 3, respectively. This is consistent with the analysis of the temperature distribution (Figure 5), which demonstrates that Case 2 is highly efficient in discharging the high-temperature gas flow out of the mining face culvert with the lowest thermal diffusion at various inlet velocities.

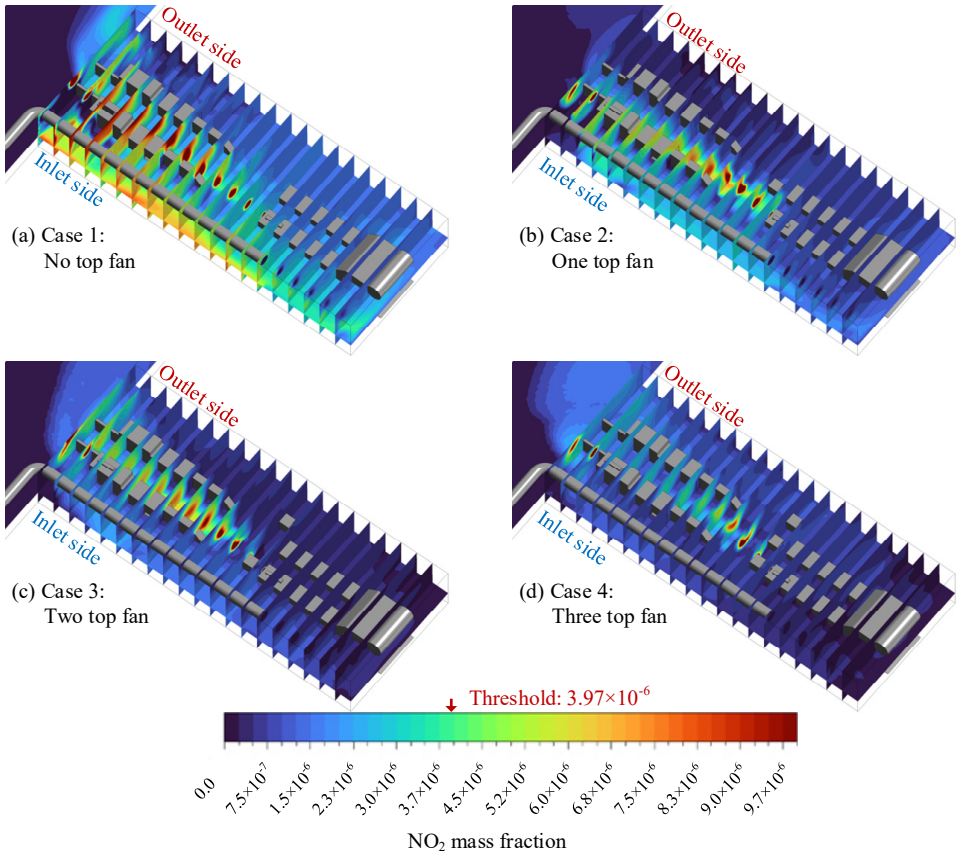


Figure 9. NO_2 mass fraction distribution for different top fan number.

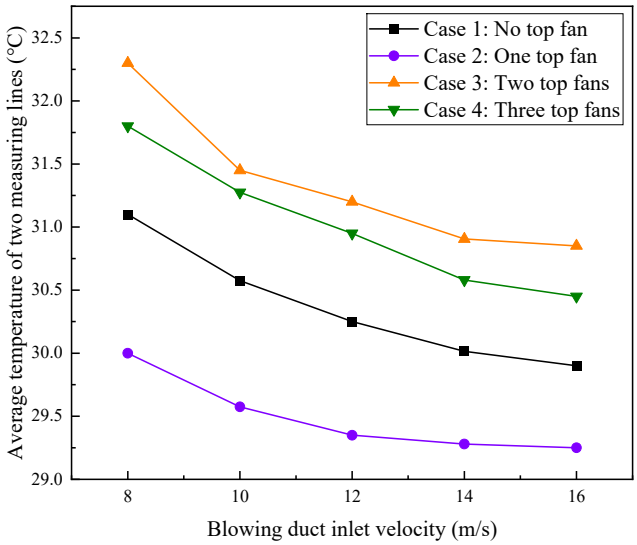
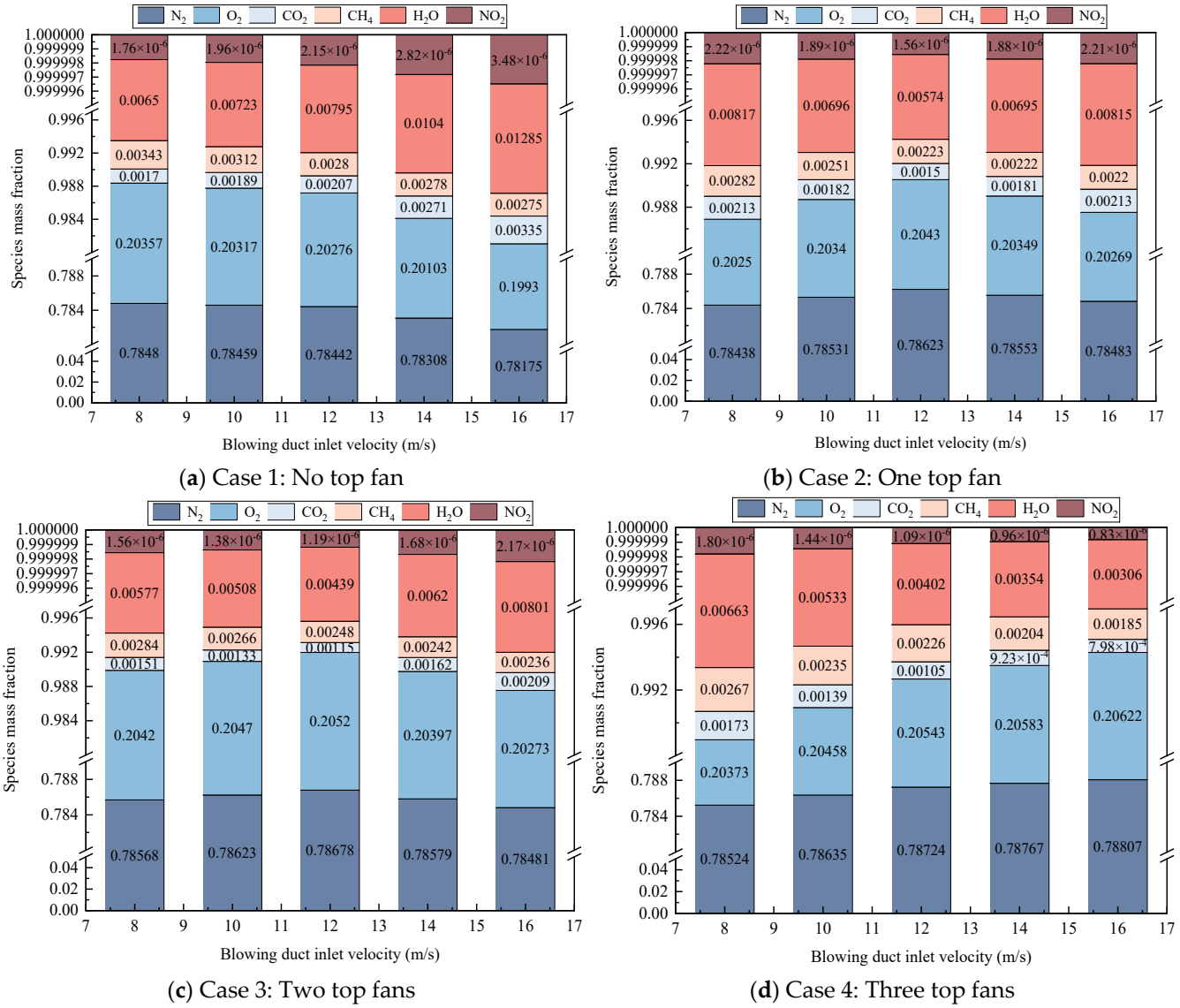


Figure 10. Impact of different blowing duct inlet velocities on the culvert temperature.

The mass fraction of each gas on the measuring lines for each of the top fan cases at different blowing duct inlet velocities is shown in Figure 11. Among the various gas components, since N_2 hardly participates in the internal reactions of the diesel engines, its mass fraction remains stable at different inlet velocities, within the range of 0.783 to 0.787. For CH_4, increasing the inlet velocity can directly increase the dilution rate of the CH_4 leaked near the mining face, so the CH_4 mass fraction decreases with an increase in the inlet velocity by different magnitudes. Case 4 shows the greatest reduction, as the inlet velocity increases from 8 m/s to 16 m/s, the CH_4 mass fraction decreases by 0.00082, followed by Cases 1, 2, and 3, where the CH_4 mass fraction decreases by 0.00068, 0.00062 and 0.00048, respectively.



(**a**) Case 1: No top fan (**b**) Case 2: One top fan

(**c**) Case 3: Two top fans (**d**) Case 4: Three top fans

Figure 11. Impact of different blowing duct inlet velocities on the species volume fraction.

For CO_2 and NO_2, there are significant differences in the patterns of variation for their mass fractions with an increase in the blowing duct inlet velocity for the different top fan cases. The CO_2 and NO_2 mass fractions in Case 1 increase monotonically with increasing inlet velocity; this is because a higher inlet velocity in Case 1 causes more fluid to flow along the outlet side, thereby reducing the dilution effect on CO_2 and NO_2. In Cases 2 and 3, the CO_2 and NO_2 mass fractions first decrease and then increase with increasing inlet velocity. This is because the top fans promote the diffusion of the fluid at the blowing

duct outlet, and increasing the inlet velocity increases the diffusion of fresh air and thus contributes to the dilution of CO_2 and NO_2. However, due to the insufficient distribution region of the fans and the inadequacy of the negative pressure at the top, an excessive inlet velocity causes the fluid to flow directly along the outlet (similar to Case 1), so the mass fractions of CO_2 and NO_2 increase. In Case 4, the mass fractions of CO_2 and NO_2 decrease monotonically. This is due to the sufficient fan distribution region and negative pressure, which ensure the effective diffusion of the fresh fluid at all inlet velocities. In addition, although the mass fraction of water vapor varies greatly from those of CO_2 and NO_2, its trend remains consistent with that of CO_2 and NO_2. This is because when the gases flow is driven by kinetic energy supply devices (top fans, the tailpipe outlet, and the blowing duct inlet), its flow and diffusion mainly depend on kinetic energy rather than gravitational potential energy.

The variation in the average temperature with the blowing duct inlet temperature for the different top fan cases is shown in Figure 12. Significantly, with an increase in the blowing duct inlet temperature, the average temperatures in all top fan cases increase. This is because a lower duct inlet temperature provides more cooling capacity to reduce the gas temperature inside the mining face culvert. In addition, Case 2 has the lowest average temperature at any duct inlet temperature, followed by Cases 1, 4, and 3, which is consistent with the relative magnitudes observed at different blowing duct inlet temperatures, and this trend is consistent with the analysis of the temperature distribution characteristics shown in Figure 5. Meanwhile, there are differences in the magnitude of the average temperature change with the blowing duct inlet temperature. For example, when the blowing duct inlet temperature increases from 5 °C to 25 °C, the average temperatures of Cases 1, 2, 3, and 4 increase by 3.30 °C, 2.30 °C, 3.45 °C and 3.50 °C, respectively. This is due to the differences in the utilization of the cooling capacity brought about by the different numbers of top fans, and this behavior is consistent with the analysis in Figure 10.

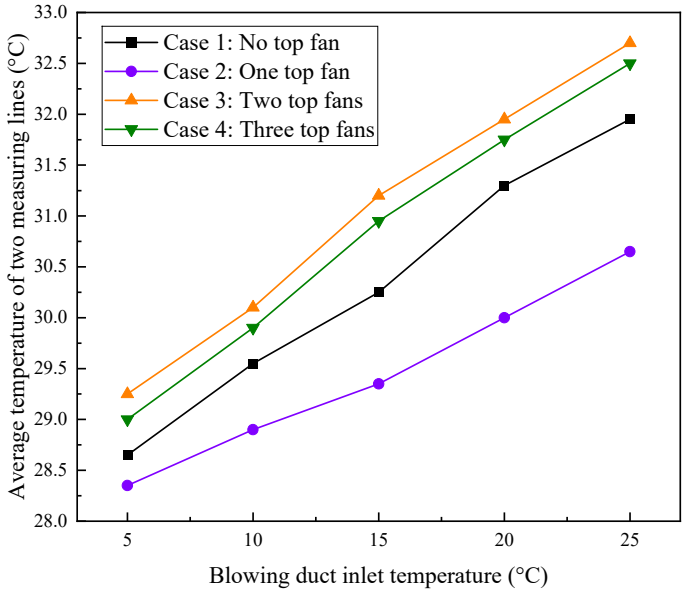
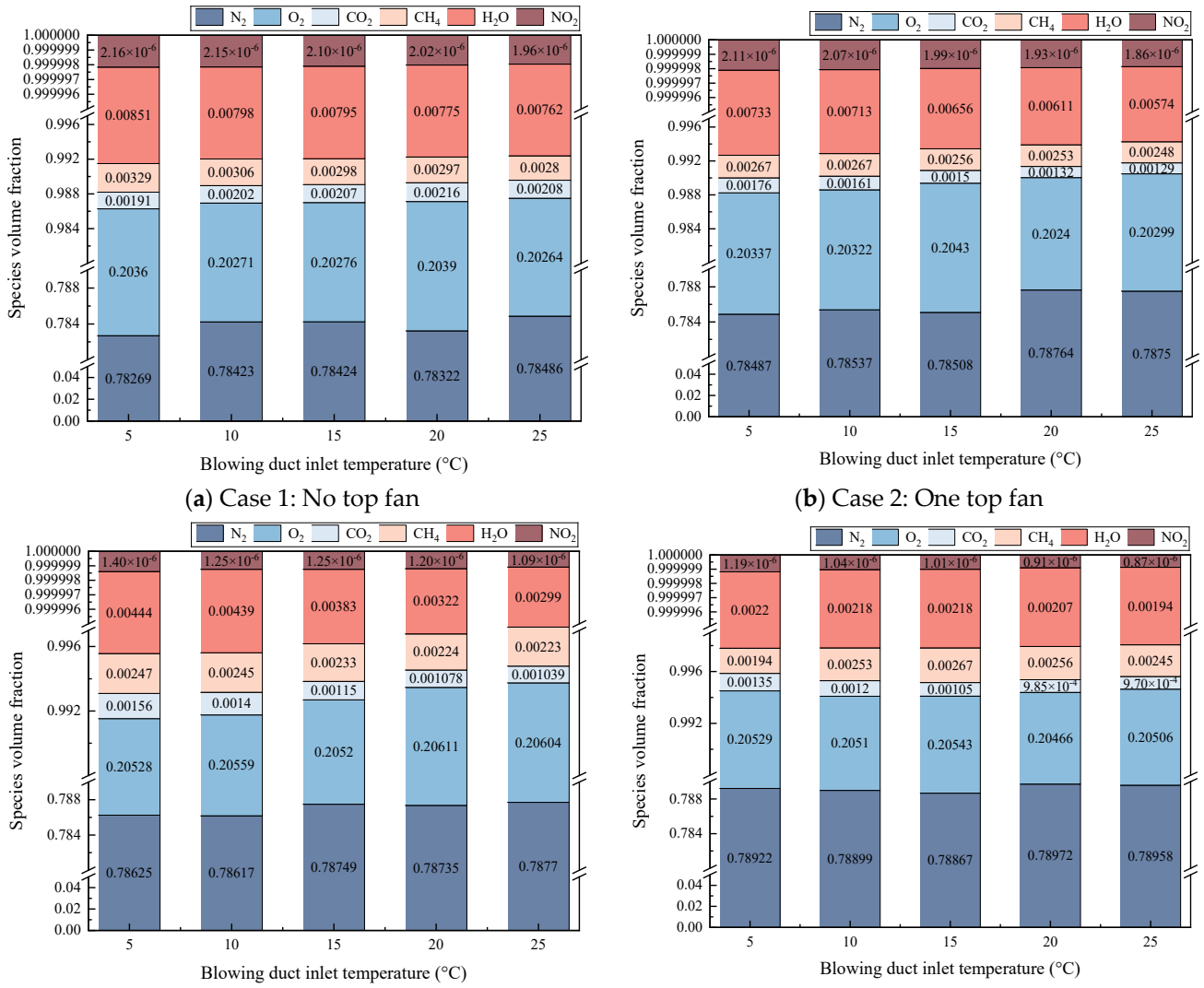


Figure 12. Impact of different blowing duct inlet temperature on the culvert temperature.

The mass fraction of each gas on the measuring lines for the top fan cases at different blowing duct inlet temperatures is shown in Figure 13. Compared to the large differences in the mass fraction of each gas due to changes in the blowing duct inlet velocity, changing the blowing duct inlet temperature does not result in a regular change in the mass fraction of each gas. For example, in Case 3, the mass fraction of O_2 is in the range of 0.2052 to 0.2062, and the mass fraction of CO_2 is in the range of 0.001309 to 0.001560. This is

because the temperature only changes the density of the different gases and thus changes the magnitude of their gravitational potential energy. However, in this study, the impact of the gravitational potential energy on the distribution of the flow field and the diffusion of the different gases is much smaller than that of the kinetic energy.



(**a**) Case 1: No top fan

(**b**) Case 2: One top fan

(**c**) Case 3: Two top fans

(**d**) Case 4: Three top fans

Figure 13. Impact of different blowing duct inlet temperature on the species volume fraction.

3.3. Comparison of Comprehensive Performance

Through the analysis in Sections 3.1 and 3.2, it is found that Case 2 has the best cooling performance, but it is much less effective than Case 3 or Case 4 in diluting hazardous gas. Accordingly, Case 4 has superior performance in diluting hazardous gases, but it contributes to the diffusion of the high-temperature flow. Meanwhile, variations in conditions such as the number of top fans, the blowing duct inlet velocity, and the temperature directly impact the magnitude of energy consumption for the ventilation system. Therefore, it is extremely necessary to propose an indicator that can provide a comprehensive evaluation of the cooling capacity, energy consumption and hazardous gas dilution capacity.

The effect of different blowing inlet velocities on the comprehensive coefficients is shown in Figure 14. In Figure 14a, the best power–temperature comprehensive coefficient is obtained for Case 2, followed by Cases 3, 4 and 1. This is because Case 2 achieves the lowest temperature with smaller fan power consumption, but for Case 1, even though the power consumption is the smallest, the excessively high temperature results in the lowest power–

temperature comprehensive coefficient. In addition, Case 2 has a slightly lower power–temperature comprehensive coefficient at higher blowing duct inlet velocities, which is due to a small temperature reduction combined with a large increase in energy consumption. In Figure 14b, increasing the number of top fans effectively increases the gas mass fraction comprehensive coefficient, which is due to the increase in the flow rate at the mining face culvert's top. However, except for Case 4, the gas mass fraction comprehensive coefficients for the other cases first increase and then decrease with the increase in the blowing duct inlet velocity; this is because the excessive velocity results in the ineffective diffusion of fresh fluid, leading to an increase in the mass fractions of carbon dioxide and nitrogen dioxide (as analyzed in Figure 11). The total comprehensive coefficients are shown in Figure 14c, and the relative magnitudes of the total comprehensive coefficients in the different cases change with an increase in the blowing duct inlet velocity; this is due to the small difference in the gas mass fractions comprehensive coefficient (maximum difference: 0.0619) at low air supply velocities, at which time the total comprehensive coefficients are dependent on the energy consumption and temperature. Correspondingly, the large difference in gas mass fraction comprehensive coefficient (maximum difference: 0.3939) at a high blowing duct inlet velocity is the main determinant of the total comprehensive coefficient.

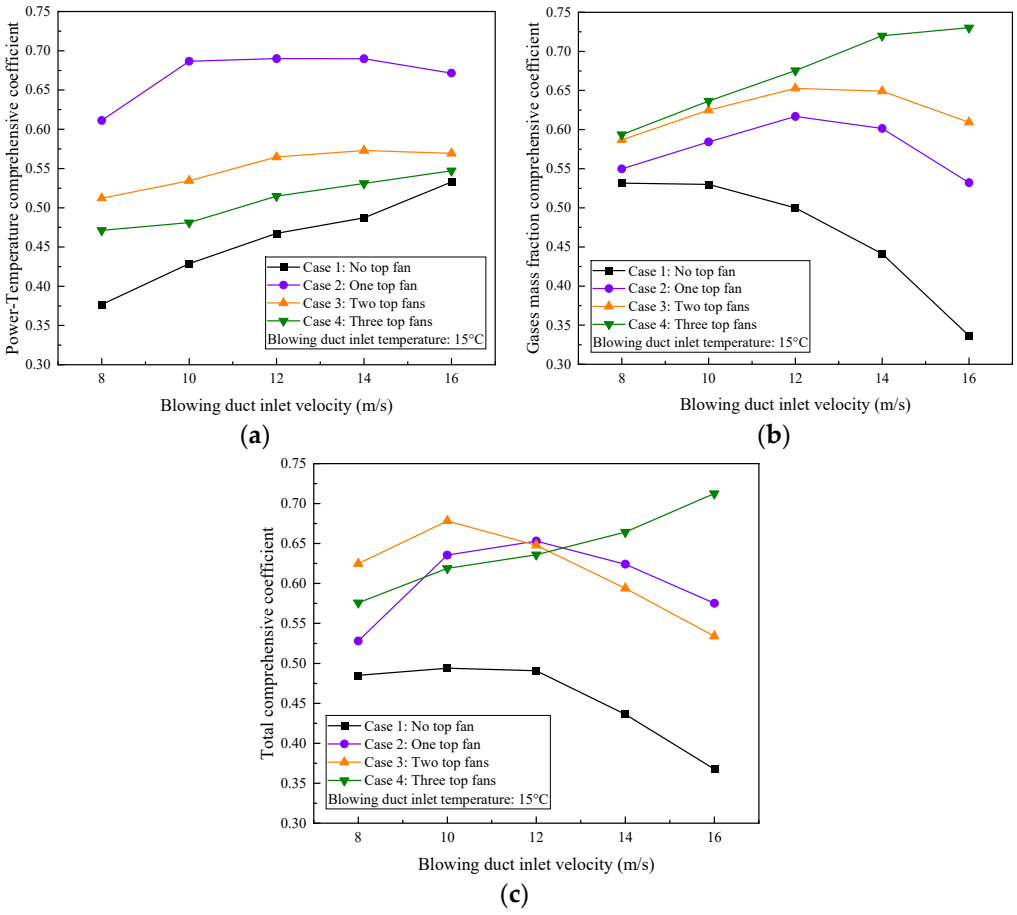


Figure 14. Impact of different blowing duct inlet temperatures on comprehensive coefficients. (**a**) Power–temperature comprehensive coefficients. (**b**) Gas mass fraction comprehensive coefficients. (**c**) Total comprehensive coefficients.

The effect of comprehensive coefficients at different blowing duct inlet temperatures is shown in Figure 14. It is easy to find that the power–temperature comprehensive coefficient in Case 2 reaches the maximum value of 0.69006 at an inlet temperature of 15 °C. This is due to the lower average temperature and lower energy consumption of Case 2 under

this condition. For the other cases, the power–temperature comprehensive coefficient decreases as the blowing duct inlet temperature increases, while the gas mass fraction comprehensive coefficient changes by a small degree, up to a maximum of only 0.20369. This is because increasing the blowing duct inlet temperature leads to a higher overall mining face culvert temperature, but its flow distribution does not notably change. How the total comprehensive coefficient varies with the inlet temperature is shown in Figure 15c. The trend of the total comprehensive coefficient in each case is consistent with that of the power–temperature comprehensive coefficient, but the relative values for each case show a large difference, resulting from the change in the relative values of the gas mass fraction.

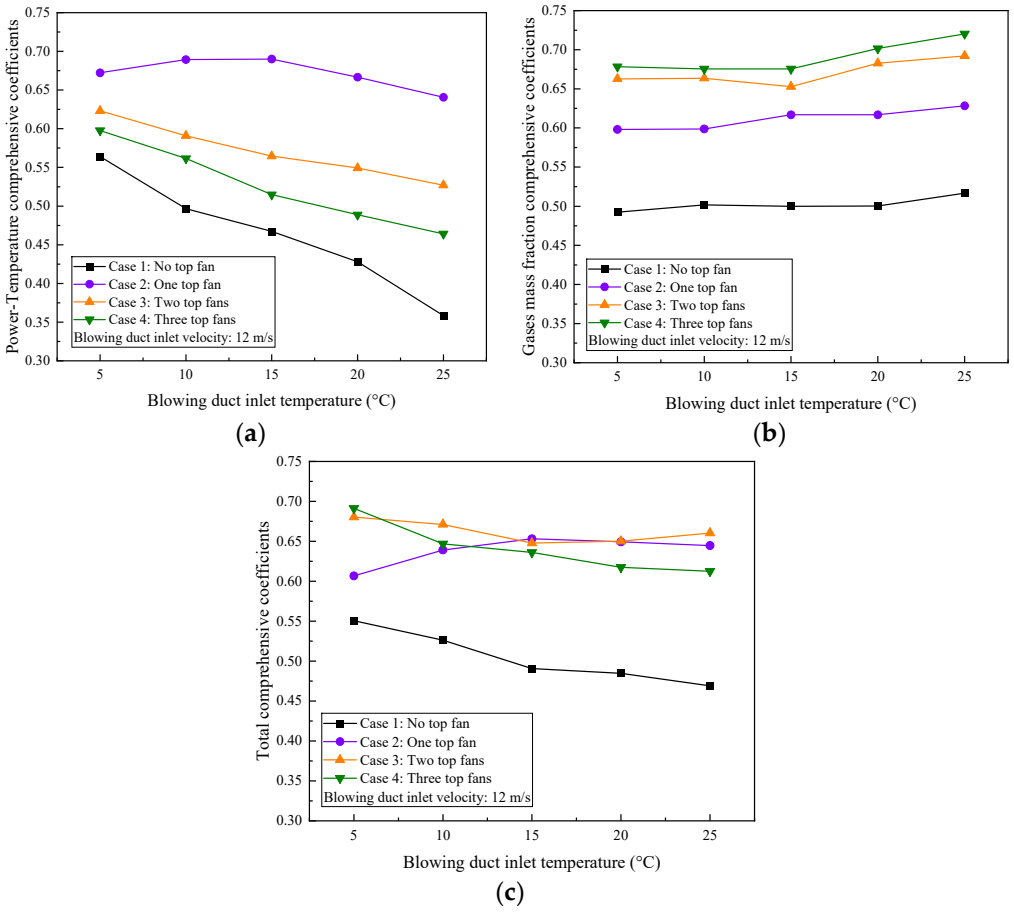


Figure 15. Impact of different blowing duct inlet velocity on comprehensive coefficients. (**a**) Power–temperature comprehensive coefficients. (**b**) Gas mass fraction comprehensive coefficients. (**c**) Total comprehensive coefficients.

4. Discussion

Based on the validated numerical simulation model of mine ventilation, this study examines the effects of the number of top fans and the blowing duct inlet conditions on the temperature, gas mass fractions, and power consumption in the mine culvert. Based on the numerical simulation results, the temperature and gas distribution characteristics are analyzed, and a comprehensive coefficient that can eliminate the influence of different indicator dimensions is proposed for assessing the ventilation performance and operational characteristics of the mine.

This study has the following limitations that need to be addressed in future research. The distance from the blowing duct inlet to the mining face is fixed at 6 m in this study. This parameter affects the diffusion range of the fresh air before it reaches the mining face and the proportion of fresh air sucked in by the top fans. A systematic sensitivity analysis of

this parameter is required to optimize the ventilation system layout. The model validation is based on a previously validated numerical model. Although the comparison shows good agreement, field experimental validation is still needed to further improve the reliability of the CFD framework, especially for the complex, turbulent, multi-species transport in deep underground mines.

Some secondary factors are neglected in this study, including radiant heat transfer, duct transmission losses and compressibility effects. Although their impact is small under the current study conditions, they may become more significant in deeper mines with higher rock temperatures and longer ventilation ducts.

Based on the current study, the following work requires further research: (1) Optimizing the distance from the blowing duct inlet to the mining face and the installation positions of the top fans to further improve the ventilation performance. (2) Conducting field experiments to validate the numerical model and calibrating the model parameters using actual mine measurement data. (3) A digital twin simulation model of the mine can be constructed by incorporating machine learning to accelerate the simulation efficiency as well as the range of working conditions. Real-time prediction of the overall temperature distribution, gas mass fraction distributions, and comprehensive coefficients can be realized based on the boundary conditions and partial measurement point data.

5. Conclusions

In this study, based on the validated numerical simulation model of the mine ventilation system, the impacts of the number of top fans and the blowing duct inlet conditions on the culvert temperature, gas mass fractions and power consumption were investigated. The performance characteristics of the mine ventilation system were evaluated using the indicators of temperature, gas mass fraction and comprehensive coefficient. Based on this study, the following conclusions can be drawn:

(1) A single top fan achieves the best cooling performance due to its low energy consumption and obtains the maximum power–temperature comprehensive coefficient (0.69006); however, it performs poorly in hazardous gas dilution, yielding a maximum gas mass fraction comprehensive coefficient of only 0.62824.
(2) Three top fans provide the maximum performance in diluting hazardous gases. Although this sacrifices some cooling capacity compared to the single top fan case, it achieves the maximum total comprehensive coefficient of 0.71246 (at a blowing inlet temperature of 15 °C, and a velocity of 16 m/s).
(3) The total comprehensive coefficients show different trends depending on the inlet conditions of the blowing duct. At low blowing duct inlet velocities, the total comprehensive coefficient is mainly affected by the energy consumption and temperature, whereas at high blowing duct inlet velocities, the difference in gas mass fraction becomes the determining factor.
(4) Different top fan cases show different sensitivities regarding cooling and hazardous gas dilution performance. This suggests that in practice, it is necessary to choose the most appropriate ventilation system configuration and operating parameters according to the specific mine environment and safety requirements, weighing the needs for temperature control, hazardous gas dilution and energy consumption.

Author Contributions: Y.L.: Conceptualization, methodology, validation, formal analysis, writing—original draft preparation. Z.Z.: Validation, formal analysis, data curation. H.W.: Reviewing and editing. Z.L. (Zhaobiao Luan): Resources, data curation. D.M.: Investigation. Q.L.: Data curation. Z.L. (Zhenneng Lu): Methodology. C.Y.: Conceptualization, methodology, software, writing—review and editing. All authors have read and agreed to the published version of the manuscript.

Funding: This research was funded by Major Project of Shandong Energy Science and Technology Plan, grant number SNKJ2022A15.

Data Availability Statement: The original contributions presented in this study are included in the article. Further inquiries can be directed to the corresponding author.

Acknowledgments: This work is supported by the Major Project of Shandong Energy Science and Technology Plan, grant number SNKJ2022A15. The financial support is sincerely appreciated.

Conflicts of Interest: Authors Yexian Liu, Zhenlei Zhu, Hongtao Wang, Zhaobiao Luan, Delong Meng, Qiang Li 1were employed by the company Shandong Energy Group Xibei Mining Co., Ltd. The remaining authors declare that the research was conducted in the absence of any commercial or financial relationships that could be construed as a potential conflict of interest.

Nomenclature

Nomenclature

c_p	Specific heat capacity at constant pressure, J/(kg·°C)
$D_{i,m}$	Mass diffusion coefficient for species in the mixture, m^2/s
$D_{T,i}$	Thermal diffusion coefficient for species in the mixture, m^2/s
g	Gravitational acceleration, m/s^2
G_κ	Turbulent kinetic energy at the mean velocity gradient, J
G_b	Turbulent kinetic energy generated by buoyancy, J
I	Unit tensor
$\vec{J}$	Diffusion flux, $Kg/(m^2 \cdot s)$
K	Motor capacity factor
M	Molar mass of mixture species, Kg/mol
y_{ij}	Normalized value of the j-th indicator
n	Number of top fans
P	Pressure, Pa
Pr	Prandtl number
Pr_t	Turbulent Prandtl number
Q	Volume flow rate, m^3/s
R	Universal gas constant
Sc_t	Turbulent Schmidt number
T	Temperature, °C
u	x direction velocity, m/s
v	y direction velocity, m/s
V	Mole volume, L/mol
w	z direction velocity, m/s
X	Mole fraction
Y	Local mass fraction

Greek symbol

β	Expansion coefficient
γ	Species mass fraction, J
ε	Dissipation rate of turbulent pulsation kinetic energy, J
η	Comprehensive coefficients
κ	Turbulent kinetic energy, J
λ	Thermal conductivity, W/(m·°C)
μ	Dynamic viscosity, Pa·s
μ_t	Turbulent viscosity, Pa·s
ω_j	Weight of each indicator
ρ	Density, kg/m^3

Abbreviations

CFD	Computational Fluid Dynamics
COP	Coefficient of cooling
GIS	Geographic information system
3D	Three-dimensional

References

1. Wang, J.; Peng, S.; Li, Y. State-of-the-Art in Underground Coal mining and Automation Technology in the United States. *J. China Coal Soc.* **2021**, *46*, 36–45.
2. Xie, H.; Zhou, H.; Xu, D.; Wang, H.; Zhang, R.; Gao, F. Research and consideration on deep coal mining and critical mining depth. *J. China Coal Soc.* **2012**, *37*, 535–542.
3. Guo, P.; Bu, M.; Zhang, P.; He, M. Research progress on the prevention and utilization of mine geothermal energy. *Chin. J. Eng.* **2022**, *44*, 1632–1651.
4. Chen, W.; Liang, S.; Liu, J. Proposed split-type vapor compression refrigerator for heat hazard control in deep mines. *Appl. Therm. Eng.* **2016**, *105*, 425–435. [CrossRef]
5. Wu, S.; Chen, S.; Guo, Y.; Huang, M.; Wu, Z.; Jiang, J.; Wu, S. The approach of heat recovery from mine exhaust airflow and efficiency enhancement: Technical analysis of wet chord grids. *Appl. Therm. Eng.* **2025**, *264*, 125423. [CrossRef]

6. Bornman, W.; Dirker, J.; Arndt, D.; Meyer, J. Integrated energy simulation of a deep level mine cooling system through a combination of forward and first-principle models applied to system-side parameters. *Appl. Therm. Eng.* **2017**, *123*, 1166–1180. [CrossRef]
7. Guo, P.; Qin, F. Preventive measures against heat hazard and its utilization in Zhangshuanglou Coal Mine. *J. China Coal Soc.* **2013**, *38*, 393–398.
8. Wang, D.; Zhang, P.; Zhang, Y.; Tu, S.; Wang, J.; Hao, Z. Distribution Characteristic and Migration Mechanism of Toxic Gases in Goafs during Close-Distance Coal Seam Mining: A Case Study of Shaping Coal Mine. *ACS Omega* **2022**, *7*, 7403–7413. [CrossRef] [PubMed]
9. Cai, P.; Nie, W.; Hua, Y.; Wei, W.; Jin, H. Diffusion and pollution of multi-source dusts in a fully mechanized coal face. *Process Saf. Environ. Prot.* **2018**, *118*, 93–105. [CrossRef]
10. He, M.; Xu, M. Research and development of HEMS cooling system and heat-harm control in deep mine. *Chin. J. Rock Mech. Eng.* **2008**, *27*, 1353–1361.
11. Xu, Y.; Li, Z.; Chen, Y.; Jia, M.; Zhang, M.; Li, R. Synergetic mining of geothermal energy in deep mines: An innovative method for heat hazard control. *Appl. Therm. Eng.* **2022**, *210*, 118398. [CrossRef]
12. Qi, Y.; Wang, M. EER test and analysis of surface ice cooling system for coal mine. *Int. J. Low-Carbon Technol.* **2020**, *15*, 382–388. [CrossRef]
13. Schutte, A.; Kleingeld, M.; Zee, L.V. An integrated energy efficiency strategy for deep mine ventilation and refrigeration. In Proceedings of the 2014 International Conference on the Eleventh industrial and Commercial Use of Energy, Cape Town, South Africa, 19–20 August 2014; pp. 1–9.
14. Wang, W.; Wang, S.; Dai, M.; Shao, K.; Cui, Z.; Liu, Y.; Shao, W.; Cheng, L. Experimental analysis on dynamic performance of refrigeration systems in a deep gold mine. *Appl. Therm. Eng.* **2022**, *217*, 119259. [CrossRef]
15. Wang, X.; Zhang, P.; Dong, X.; Wang, J.; Fang, J.; Zhang, X.; Liu, L. Numerical research on geothermal energy extraction in backfilled mines by using the excellent heat transfer performance of loop heat pipe. *Int. Commun. Heat Mass Transf.* **2025**, *160*, 108385. [CrossRef]
16. Bascompta, M.; Castañón, A.; Sanmiquel, L.; Oliva, J. A GIS-based approach: Influence of the ventilation layout to the environmental conditions in an underground mine. *J. Environ. Manag.* **2016**, *182*, 525–530. [CrossRef] [PubMed]
17. Chen, X.; Zhang, Y.; Ji, J.; Miao, D. Ventilation and cooling of coal mining face based on CFD model optimization. *Process Saf. Environ. Prot.* **2023**, *172*, 746–777. [CrossRef]
18. Wang, J.; Jiang, C.; Zhou, X.; Kang, J.; Yu, S.; Bai, G. Head-neck local ventilation mode for long-narrow mine working face. *Sci. Rep.* **2024**, *14*, 19663. [CrossRef] [PubMed]
19. Habibi, A.; Kramer, R.; Gillies, A. Investigating the effects of heat changes in an underground mine. *Appl. Therm. Eng.* **2015**, *90*, 1164–1171. [CrossRef]
20. Kurnia, J.; Sasmito, A.; Wong, W.; Mujumdar, A. Prediction and innovative control strategies for oxygen and hazardous gases from diesel emission in underground mines. *Sci. Total Environ.* **2014**, *481*, 317–334. [CrossRef] [PubMed]
21. Ministry of Emergency Management of the People's Republic of China, Coal Mine Safety Regulations 2016. Available online: https://www.mem.gov.cn/gk/gwgg/agwzlfl/zjl_01/201603/t20160325_233784.shtml (accessed on 26 February 2025).
22. Pinna, F.; Zucca, M.; Simoncelli, M.; Stochino, F. A new logarithmic congestion model for vent sizing and reduced pressure prediction in baghouse dust collectors. *J. Loss Prev. Process Ind.* **2025**, *99*, 105829. [CrossRef]
23. *MT 220-1990*; Coal Mine Explosion-Proof Diesel Engine Exhaust Carbon Monoxide Nitrogen Oxides Inspection Specification. National Energy Administration of China: Beijing, China, 1990.

Disclaimer/Publisher's Note: The statements, opinions and data contained in all publications are solely those of the individual author(s) and contributor(s) and not of MDPI and/or the editor(s). MDPI and/or the editor(s) disclaim responsibility for any injury to people or property resulting from any ideas, methods, instructions or products referred to in the content.